Journal of Computational and Applied Mathematics 234 (2010) 2377–2389

Contents lists available at ScienceDirect

Journal of Computational and Applied Mathematics

journal homepage: www.elsevier.com/locate/cam

Grid structure impact in sparse point representation of derivatives

Margarete O. Domingues [a], Paulo J.S.G. Ferreira [e,f], Sônia M. Gomes [b,c,*], Anamaria Gomide [b,d], José R. Pereira [e,g], Pedro Pinho [g,h]

[a] *Laboratório Associado de Computação e Matemática Aplicada (LAC), Cordenação dos Laboratórios Associados(CTE), Instituto Nacional de Pesquisas Espaciais (INPE), Av. dos Astronautas, 1758, 12227-010 São José dos Campos, Brazil*

[b] *Universidade Estadual de Campinas, Brazil*

[c] *IMECC- Rua Sérgio Buarque de Holanda, 651 - Cidade Universitária CEP 13083-859, Campinas, SP, Brazil*

[d] *IC, Caixa Postal 6176, 13074-971 Campinas, SP, Brazil*

[e] *Universidade de Aveiro, Portugal*

[f] *DETI/IEETA, Campus Universitário de Santiago, 3810-193 Aveiro, Portugal*

[g] *Instituto Tecnológico, Campus Universitário de Santiagao, 3810-193 Aveiro, Portugal*

[h] *Instituto Superior de Engenharia de Lisboa. Rua Conselheiro Emidio Navarro, 1, 1950-062 Lisboa, Portugal*

ARTICLE INFO

Article history:
Received 19 December 2008
Received in revised form 21 January 2010

MSC:
42C40
65M06
65M50

Keywords:
Wavelets
Multiresolution analysis
Adaptivity
Sparse grids
Finite differences
Consistency analysis

ABSTRACT

In the Sparse Point Representation (SPR) method the principle is to retain the function data indicated by significant interpolatory wavelet coefficients, which are defined as interpolation errors by means of an interpolating subdivision scheme. Typically, a SPR grid is coarse in smooth regions, and refined close to irregularities. Furthermore, the computation of partial derivatives of a function from the information of its SPR content is performed in two steps. The first one is a refinement procedure to extend the SPR by the inclusion of new interpolated point values in a security zone. Then, for points in the refined grid, such derivatives are approximated by uniform finite differences, using a step size proportional to each point local scale. If required neighboring stencils are not present in the grid, the corresponding missing point values are approximated from coarser scales using the interpolating subdivision scheme. Using the cubic interpolation subdivision scheme, we demonstrate that such adaptive finite differences can be formulated in terms of a collocation scheme based on the wavelet expansion associated to the SPR. For this purpose, we prove some results concerning the local behavior of such wavelet reconstruction operators, which stand for SPR grids having appropriate structures. This statement implies that the adaptive finite difference scheme and the one using the step size of the finest level produce the same result at SPR grid points. Consequently, in addition to the refinement strategy, our analysis indicates that some care must be taken concerning the grid structure, in order to keep the truncation error under a certain accuracy limit. Illustrating results are presented for 2D Maxwell's equation numerical solutions.

1. Introduction

The Sparse Point Representation (SPR) method is an adaptive finite difference strategy introduced in [1] to calculate numerical solutions of partial differential equations (PDE) constrained by initial and boundary conditions. Our goal in this paper is to show how the truncation error in the SPR evaluation of partial derivatives can be controlled, by regarding possible perturbations coming from the presence of irregular grids and the use of local scales as the step size.

* Corresponding author at: IMECC- Rua Sérgio Buarque de Holanda, 651 - Cidade Universitária CEP 13083-859, Campinas, SP, Brazil.
E-mail addresses: margarete@lac.inpe.br (M.O. Domingues), pjf@ieeta.pt (P.J.S.G. Ferreira), soniag@ime.unicamp.br (S.M. Gomes), anamaria@ic.unicamp.br (A. Gomide), jrp@det.ua.pt (J.R. Pereira), ppinho@deetc.isel.ipl.pt (P. Pinho).

0377-0427/$ – see front matter © 2010 Elsevier B.V. All rights reserved.
doi:10.1016/j.cam.2010.02.035

The SPR method combines the simplicity and accuracy of traditional finite difference schemes with the ability of wavelet coefficients in the characterization of local regularity of functions. In this sense, the method has two basic parts: the operational part, and the representation part. In the operational part, the background context is of an accurate and stable finite difference scheme L^j_{FD} in a uniform grid X^j. In the representation part, the tools come from interpolating wavelet analysis. The data is organized by levels of resolution $0 \leq \ell \leq j$, j being the finest scale level. In such a multilevel context, the key role is played by interpolating subdivision schemes, which are the basis for the definition of reconstruction operators, wavelet coefficients being precisely the interpolation errors at the new points occurring when going from one level of discretization to the next finer one. In the construction of SPR grids, the idea is to use the wavelet coefficients as indicators of the local smoothness of the solution. This is the main ingredient in the definition of the thresholding operator: only those points corresponding to wavelet coefficients of magnitude greater than a prescribed threshold ϵ should be kept in the adaptive grid $\Gamma^j_\epsilon \subset X^j$. A reduced number of points are found in Γ^j_ϵ, the grid being less refined in regions where the variation of the function is smooth. For PDE simulations in SPR grids, the scheme considers an adaptive finite difference version L^j_a. Even though the grid spacing in a SPR grid is not uniform, at each of its points the FD formula is applied using a uniform step size. Since required neighboring stencils may not be present in the grid, such missing point values are approximated from coarser scales by the interpolating subdivision scheme of the same order. Two aspects of this SPR scheme should be emphasized. Firstly, the rule is to choose the step size proportional to each point local scale. The goal is to be more economical, in terms of the number of operations to be done, than the procedure of calculating the stencils up to the most refined level. In fact, for those points in smooth regions with wide local scales, the number of stencil interpolations required for the application of L^j_a may be significantly reduced. Secondly, the SPR grid of a function may not be convenient for the SPR representation after the application of the finite difference operator. Therefore, before the application of L^j_a, the SPR grid should be refined by the inclusion of a security zone of new (interpolated) point values.

For this adaptive finite difference strategy, a generalization of the concept of truncation error, which is the familiar basis of the analysis of difference schemes, is presented in [2] for unidimensional domains and for schemes of arbitrary orders. In the present paper, we extend the consistency analysis in [2] to bidimensional domains, for the particular case of the cubic interpolating subdivision scheme, and of fourth order FD discretizations of partial derivatives $L^r f = \frac{\partial f}{\partial r}$, $r \in \{x, y\}$. The purpose is to analyse the effect of using the directional local scale in the SPR scheme $L^{r,j}_a$ instead of computing the FD formula with the spacing of the finest scale level.

The sections of the present paper are organized as follows. In Section 2, we describe the main wavelet tools required for the representation part of the SPR method. In Section 3 we prove some results concerning the local behavior of the reconstruction operators, which stand for SPR grids holding appropriate directional local scales. We show that for grids having a certain tree structure it is possible to define such directional local scales properly. Section 4 is dedicated to the study of SPR adaptive finite difference schemes $L^{r,j}_a$. Firstly, in combination with the local behavior of the reconstruction operators, it is shown that $L^{r,j}_a$ can be formulated in terms of a collocation scheme based on the wavelet expansion associated to the SPR. This fact implies that the SPR derivative can give the same result either using the point directional local scale as step size or using the spacing of the finest scale level. Consequently, the consistency analysis indicates that, in order to keep the truncation error under a certain accuracy limit, some care must be taken concerning two aspects. In addition to a reliable refinement strategy, it is also important to have an appropriate definition of the directional local scale which holds for certain grid structures. In Section 5, we present some illustrating examples of SPR derivatives for magnetic fields arising in the numerical simulation of 2D Maxwell's equations. Concluding remarks are included in Section 6.

2. Multiresolution analysis on irregular grids

As explained before, our goal in this paper is to show how the truncation error can be controlled, regarding possible perturbations coming from the application of an adaptive SPR scheme. Before going to this point in the following sections, we shall describe here the required tools from wavelet analysis in more detail.

In a multiscale framework, functions are represented in different scale levels, and the main tools are appropriate transformations relating the information at the finest scale level j to the lower ones, and vice versa. In the context of interpolating multiresolution analyses, the input data f^j contains the sample values at a grid on the finest scale level. After a transformation WT^j, the output contains the information f^0 in the coarsest level, and d^ℓ that keeps the details between a scale level ℓ and the next upper level $\ell + 1$. Schematically, we have

$$f^j \overset{WT^j}{\rightarrow} f^j_{MR} = (f^0, d^0, \ldots, d^{j-1}).$$

In a uniform setting in 2D, each scale level ℓ corresponds to a uniform grid X^ℓ. Starting from X^0, the grid at the coarsest level with spacings Δ^0_x in the x-direction and Δ^0_y in the y direction, the hierarchy of uniform grids X^ℓ, $\ell \geq 1$ is

$$X^\ell = \left\{\gamma = (k\Delta^\ell_x, m\Delta^\ell_y),\ 0 \leq k \leq N^\ell_x,\ 0 \leq m \leq N^\ell_y\right\},$$

where $\Delta^\ell_x = 2^{-\ell}\Delta^0_x$ and $\Delta^\ell_y = 2^{-\ell}\Delta^0_y$. As indicated in Fig. 1, its dyadic refinement $X^{\ell+1}$,

$$X^{\ell+1} = \left\{\gamma = (k\Delta^{\ell+1}_x, m\Delta^{\ell+1}_y),\ 0 \leq k \leq 2N^\ell_x,\ 0 \leq m \leq 2N^\ell_y\right\},$$

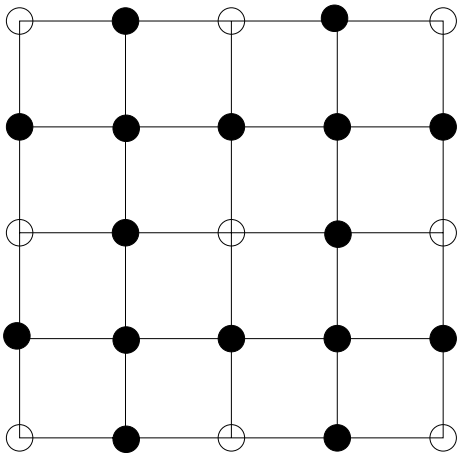

Fig. 1. Uniform dyadic grids: ∘- points in X^ℓ, •- points in $X^{\ell+1} \setminus X^\ell$.

is obtained by the inclusion of new midpoints $\gamma = (2k\Delta_x^{\ell+1}, (2m+1)\Delta_y^{\ell+1})$, $\gamma = ((2k+1)\Delta_x^{\ell+1}, 2m\Delta_y^{\ell+1})$, and $\gamma = ((2k+1)\Delta_x^{\ell+1}, (2m+1)\Delta_y^{\ell+1})$.

In a non-uniform setting, the principle is also to have the information data hierarchically organized by different levels of resolution. On this matter, we are concerned with a sequence of embedded grids $\Gamma^\ell \subset \Gamma^{\ell+1}$. It shall be assumed that $\Gamma^0 = X^0$. For $\ell \geq 0$, $\Gamma^{\ell+1} \subset X^{\ell+1}$ is constructed from Γ^ℓ by including some new points of $X^{\ell+1} \setminus X^\ell$. We shall denote by Λ^ℓ the set of such new points in $\Gamma^{\ell+1} \setminus \Gamma^\ell$.

Let $f^\ell = (f_\gamma^\ell)$ be the set of sample values labeled by the points $\gamma \in \Gamma^\ell$. As described in the following algorithms, for the definition of WT^j and its inverse $(WT^j)^{-1}$, the main ingredients are reconstruction interpolation operators $\mathcal{R}^\ell(\nu; f^\ell)$ that predict $f(\nu)$ at any location ν from the knowledge of its discrete sample values f^ℓ at Γ^ℓ. The wavelet coefficients d_γ^ℓ are defined for points $\gamma \in \Lambda^\ell$ as the errors in this prediction.

Analysis - $f^j \overset{WT^j}{\to} (f^0, d^0, \ldots, d^{j-1})$

- *For* $\ell = j-1, \ldots, 0$
  Define $f_\gamma^\ell = f_\gamma^{\ell+1}$ if $\gamma \in \Gamma^\ell$
  If $\gamma \in \Lambda^\ell$, *calculate* $\tilde{f}_\gamma^{\ell+1} = \mathcal{R}^\ell(\gamma, ; f^\ell)$, *and set* $d_\gamma^\ell = f_\gamma^{\ell+1} - \tilde{f}_\gamma^{\ell+1}$

Synthesis - $(f^0, d^0, \ldots, d^{j-1}) \overset{(WT^j)^{-1}}{\to} f^j$

- *For* $\ell = 0, \ldots, j-1$
  Define $f_\gamma^{\ell+1} = f_\gamma^\ell$ if $\gamma \in \Gamma^\ell$
  If $\gamma \in \Lambda^\ell$, *calculate* $\tilde{f}_\gamma^{\ell+1} = \mathcal{R}^\ell(\gamma; f^\ell)$ *and set* $f_\gamma^{\ell+1} = d_\gamma^\ell + \tilde{f}_\gamma^{\ell+1}$.

Reconstruction interpolation operators

For input data f^ℓ sampled at uniform grids X^ℓ, the definition of the interpolation operator $\mathcal{R}^\ell(\nu, f^\ell)$, at any point ν, uses a classical interpolation subdivision scheme, which is done iteratively, as suggested in [3]. On the first step, we set $\mathcal{R}^\ell(\nu; f^\ell) = f_\nu^\ell$, $\nu \in X^\ell$. Having $\mathcal{R}^\ell(\nu; f^\ell)$ being defined for all $\nu \in X^q$, $q \geq \ell$, then the definition is refined to X^{q+1} by means of an interpolating prediction operator $P_q^{q+1} : s^q \to s^{q+1}$, where $s^q = (s_{k,m}^q)$ and $s^{q+1} = (s_{k,m}^{q+1})$ are sequences labeled according to the points $(k\Delta_x^q, m\Delta_y^q) \in X^q$ and $(k\Delta_x^{q+1}, m\Delta_y^{q+1}) \in X^{q+1}$, respectively. For other non dyadic points, the definition is set by a limit procedure.

For non-uniform grids $\Gamma^\ell \subsetneq X^\ell$, the definition of the interpolation operators $\mathcal{R}^\ell(\nu; f^\ell)$ uses a simple modification of the classical interpolation subdivision scheme, as introduced in [4]. On the coarsest level, we set $\mathcal{R}^\ell(\nu; f^\ell) = f_\nu^0$, $\nu \in X^0$. Having $\mathcal{R}^\ell(\nu; f^\ell)$ being defined for all $\nu \in X^q$, $0 \leq q < \ell$, then the definition is extended to $X^{q+1} \setminus \Gamma^\ell$ by means of the prediction interpolation scheme P_q^{q+1}, and it is set $\mathcal{R}^\ell(\nu; f^\ell) = f_\nu^\ell$, if $\nu \in \Gamma^\ell \cap X^{q+1}$. For points $\nu \in X^q$, $q > \ell$, the definition is set as in the classical subdivision scheme. Consequently, for practical implementations of the analysis and synthesis algorithms the crucial ingredient is the prediction operator P_q^{q+1}, which is iteratively used in the formulation of the reconstruction operator $\mathcal{R}^\ell$.

For linear prediction operators P_q^{q+1}, the reconstruction operators $\mathcal{R}^\ell(\nu; f^\ell)$ can be expressed as $\mathcal{R}^\ell(\nu; f^\ell) = \sum_{\gamma \in \Gamma^\ell} f_\gamma^\ell \Phi_\gamma^\ell(\nu)$, where $\Phi_\gamma^\ell(\nu) = \mathcal{R}^\ell(\nu; \delta^\ell)$ is the reconstruction of the delta-sequence $\delta_\gamma^\ell = \delta(\eta - \gamma)$, $\eta \in \Gamma^\ell$. Therefore, Φ_γ^ℓ satisfies the interpolatory property $\Phi_\gamma^\ell(\eta) = \delta(\eta - \gamma)$, $\eta \in \Gamma^\ell$. From its definition, the reconstruction operators can

also be expressed as

$$\mathcal{R}^\ell(\nu; f^\ell) = \sum_{\gamma \in X^\ell} \tilde{f}^\ell_\gamma \phi^\ell_\gamma(\nu), \tag{1}$$

where $\tilde{f}^\ell_\gamma = f_\gamma$ if $\gamma \in \Gamma^\ell$, and $\tilde{f}^\ell_\gamma = \mathcal{R}^\ell(\gamma; f^\ell)$ if $\gamma \in X^\ell \setminus \Gamma^\ell$, and $\phi^\ell_\gamma(\nu)$ are the interpolatory scaling functions for the uniform grid case $\Gamma^\ell = X^\ell$. Furthermore, it can be proved that the multilevel wavelet representation holds

$$\mathcal{R}^\ell(\nu; f^\ell) = \sum_{\gamma \in X^{j_0}} f^0_\gamma \phi^0_\gamma(\nu) + \sum_{\ell=0}^{j-1} \sum_{\gamma \in \Lambda^l} d^\ell_\gamma \psi^\ell_\gamma(\nu), \tag{2}$$

where $\psi^\ell_\gamma(\nu) = \phi^\ell_\gamma(\nu)$, $\nu \in \Lambda^\ell$. Under this functional point of view, the transformations $f^j \leftrightarrow (f^0, d^0, \ldots, d^{j-1})$ correspond to the change between the basis $\{\Phi^j_\gamma, \gamma \in \Gamma^j\}$ and $\{\phi^0_\gamma, \gamma \in X^0\} \cup \{\psi^0_\gamma, \gamma \in \Lambda^0\} \cup \ldots \cup \{\psi^{j-1}_\gamma, \gamma \in \Lambda^{j-1}\}$. In the case of uniform grids X^j, this interpolating wavelet approach was introduced in [5]. In the context of nonuniform grids, it was first considered in [4], and then extended in [6] to discretizations by cell averages on the interval.

SPR method

In the above discussion, multiresolution analyses for point values on a pre-established irregular grid have been considered. The connection between the grid and the particular function under analysis has not been covered. However, in wavelet analysis this kind of irregular grid appears after the thresholding of wavelet coefficients. Therefore, different grids are usually associated to distinct functions and threshold parameters. The terminology *Sparse Point Representation* introduced in [1] is related to this kind of mapping between functions and grid point values.

As interpolation errors, the wavelet coefficients can be used as indicators of local smoothness. Indeed, suppose that a connected region $\mathcal{N}$, with diameter $\lesssim 2^{-\ell}$, contains $\gamma \in \Lambda^\ell$ and the corresponding interpolating points required for the computation of d^ℓ_γ. Suppose also that the function f presents a regularity σ in a Sobolev space $\mathcal{W}^{\sigma,\infty}(\mathcal{N})$, $1 \le \sigma \le 2p$. Then,

$$\begin{aligned} |d^\ell_\gamma| &\le \inf_{g \in \mathcal{P}_{\sigma-1}} \max_{\nu \in \mathcal{N}} |f(\nu) - g(\nu)| \\ &\lesssim 2^{-\ell\sigma} \|f\|_{\mathcal{W}^{\sigma,\infty}(\mathcal{N})}, \end{aligned}$$

where $\mathcal{P}_{\sigma-1}$ is the space of the polynomial with degree less or equal $\sigma - 1$. This fact leads to the definition of a point index $i_\varepsilon(\gamma)$ which is based on the significance of the wavelet coefficients associated to γ, as compared to a certain given threshold ε. Therefore, according to these principles, the point index i_ε is defined by

$$i_\varepsilon(\gamma) = \begin{cases} 0 & \text{if } |d^\ell_\gamma| \le \varepsilon \quad \text{for } \gamma \in \Lambda^\ell \\ 1 & \text{otherwise.} \end{cases}$$

This isthe main ingredient in the definition of the thresholding operator $\mathcal{T}_\varepsilon$.

Thresholding operator (grid coarsening) $\Gamma^j \xrightarrow{\mathcal{T}_\epsilon} \Gamma^j_\varepsilon$

- If $i_\varepsilon(\gamma) = 1$, keep γ in the adapted grid Γ^j_ε.
- If $i_\varepsilon(\gamma) = 0$, remove γ from the adapted grid Γ^j_ε.

This procedure led to sparse representations $f^j_{SPR,\varepsilon} = (f^j_\gamma, \gamma \in \Gamma^j_\varepsilon)$ where only the sample values required to reconstruct f^j with error less than ε are retained.

A note about the notation

In applications of this paper, there are several grids involved, with discretizations and reconstructions operators associated to them, and thus several multiresolution analyses. It is useful to keep a unified notation for most of the operations involved, independently of which sparse grid the discretization and reconstruction operators are associated with. For instance, we have already used the convenient notation $\tilde{f}^j_\gamma = \mathcal{R}^j(\gamma; f^j)$, $\gamma \notin \Gamma^j$. Similarly, the multiresolution transform, and the thresholding operators are persistently referred to as WT^j and $\mathcal{T}_\varepsilon$, independently of the multiresolution analysis at hand. It is clear that always $\mathcal{T}_\varepsilon f^j = \mathcal{T}_\varepsilon \tilde{f}^j$.

3. Local behavior of the reconstruction operators

From hereon, we shall be concerned with the case of multiresolution analysis corresponding to the prediction operator defined by central cubic polynomial interpolation.

Cubic interpolating prediction operator P^{q+1}_q

- At the old points $\nu = (2k\Delta^{q+1}_x, 2m\Delta^{q+1}_y) \in X^q$, define $s^{q+1}_{2k,2m} = s^q_{k,m}$.

- At the new points $\nu \in X^{q+1} \setminus X^q$, use the formulae

$$s^{q+1}_{2k,2m+1} = \sum_n h(2n+1) s^q_{k,m-n},$$
$$s^{q+1}_{2k+1,2m} = \sum_n h(2n+1) s^q_{k-n,m},$$
$$s^{q+1}_{2k+1,2m+1} = \sum_n h(2n+1) s^{q+1}_{2k,2m-2n+1},$$

where the coefficients $h(n)$ are symmetric $h(-n) = h(n)$ and vanish for even integers $n \neq 0$ and all integers such that $|n| \geq 4$. The non vanishing coefficients are $h(0) = 1$, $h(1) = h(-1) = 9/16$ and $h(3) = h(-3) = -1/16$.

For the definition of SPR discretizations of partial derivatives, we need the concept of directional local scales $a^j_r(\gamma) > 0$, $\gamma \in \Gamma^j$, where $r \in \{x, y\}$. We have particular interest in directional local scales satisfying the following conditions.

Local scale conditions

(A) There is some $0 \leq q \leq j$ such that $a^j_r(\gamma) = \Delta^q_r$.
(B) If $a^j_r(\gamma) = \Delta^q_r$, then $\gamma \in \Gamma^q$.
(C) If $\gamma \in \Lambda^\ell$, then $a^j_r(\gamma) \leq \Delta^{\ell+1}_r$, $0 \leq \ell \leq j-1$.

Under such conditions, we shall prove the following local behavior of the reconstructions $\mathcal{R}^j(\nu; f^j)$ close to a point $\gamma \in \Gamma^j$, which is the basis for the consistency analysis of the next section.

Lemma 1. *Let us consider reconstructions operators based on a cubic interpolating prediction for a nonuniform grid Γ^j. Suppose that at each point in Γ^j we have defined directional local scales satisfying conditions (A–C). Let $\gamma = (\gamma_x, \gamma_y) \in \Gamma^j$ be such that, for $r \in \{x, y\}$, $a^j_r(\gamma) = \Delta^q_r$, $q = q(\gamma, r) \leq j$. Then $\forall \nu \in S^\ell_r(\gamma)$, $q \leq \ell \leq j$,*

$$\mathcal{R}^q(\nu; f^q) = \mathcal{R}^j(\nu; f^j),$$

where

$$S^\ell_x(\gamma) = \{\nu = (\gamma_x + k\Delta^\ell_x, \gamma_y), |k| \leq 2\}$$

and

$$S^\ell_y(\gamma) = \{\nu = (\gamma_x, \gamma_y + m\Delta^\ell_y), |m| \leq 2\}.$$

Proof. By construction, $\mathcal{R}^j(\nu; f^j)$ and $\mathcal{R}^q(\nu; f^q)$ coincide on X^q. By condition (B), we know that $\gamma \in \Gamma^q$. Then $S^q_x(\gamma) \subset X^q$, and thus the assertion is true for $\ell = q$. The proof advances by induction for $\ell \geq q+1$. Let $r = x$. For $\nu = (\gamma_x \pm 2\Delta^\ell_x, \gamma_y) \in S^{\ell-1}_x(\gamma)$, we already know that the result is true from the previous step. The points $\nu = (\gamma_x \pm \Delta^\ell_x, \gamma_y) \in \Lambda^{\ell-1}$ are not in Γ^j. Indeed, if $\nu \in \Gamma^j$, condition (C) implies that $a^j_x(\gamma) \leq \Delta^\ell_x < \Delta^q_x$, which is a contradiction. Consequently, $\mathcal{R}^j(\nu; f^j)$ and $\mathcal{R}^q(\nu; f^q)$ are obtained by cubic interpolation from their corresponding values at the four points in $X^{\ell-1}$ closest to ν in the x-direction. For $\nu = (\gamma_x - \Delta^\ell_x, \gamma_y)$, the interpolation points are

$$(\gamma_x - 2\Delta^{\ell-1}_x, \gamma_y), \quad (\gamma_x - \Delta^{\ell-1}_x, \gamma_y), \quad (\gamma_x, \gamma_y) \quad \text{and} \quad (\gamma_x + \Delta^{\ell-1}_x, \gamma_y).$$

For $\nu = (\gamma_x + \Delta^\ell_x, \gamma_y)$, the interpolation points are

$$(\gamma_x - \Delta^{\ell-1}_x, \gamma_y), \quad (\gamma_x, \gamma_y), \quad (\gamma_x + \Delta^{\ell-1}_x, \gamma_y) \quad \text{and} \quad (\gamma_x + 2\Delta^{\ell-1}_x, \gamma_y).$$

In both cases, the result of the previous induction step implies that $\mathcal{R}^j(.; f^j)$ and $\mathcal{R}^q(.; f^q)$ coincide at the interpolation points. Therefore, they coincide at ν as well. The proof for the stencil points in the vertical direction is similar. □

As indicated in [2], to prove a similar result for one dimensional reconstruction operators based on polynomial interpolation of higher degrees, in addition to conditions (A–C), the size of the stencils $S^\ell_r(\gamma)$ should be wider and other requirements should be satisfied. The generalization of such conditions to higher dimensions is an open question.

Example

For $\gamma = (\gamma_x, \gamma_y) \in \Gamma^j$, let us consider the following directional local scales $a^j_r(\gamma)$, $r \in \{x, y\}$:

$$a^j_x(\gamma) = \min\{\Delta^q_x, |\gamma_x - \eta_x|, \eta = (\eta_x, \gamma_y) \in \Gamma^j, \eta \neq \gamma\} \tag{3}$$
$$a^j_y(\gamma) = \min\{\Delta^q_y, |\gamma_y - \eta_y|, \eta = (\gamma_x, \eta_y) \in \Gamma^j, \eta \neq \gamma\}, \tag{4}$$

where $q = 0$ for $\gamma \in X^0$, and $q = \ell + 1$ for $\gamma \in \Lambda^\ell$, $0 \leq \ell \leq j-1$.

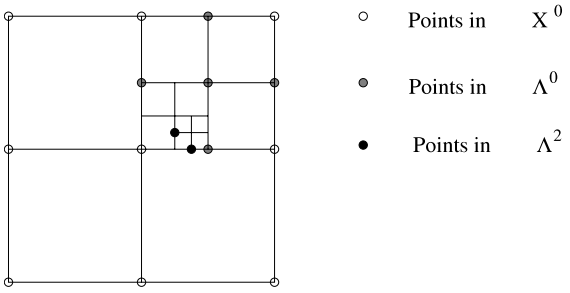

Fig. 2. Example of grid for which the local scale (3) does not fulfill the condition (A).

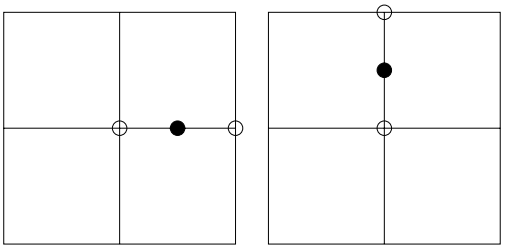

Fig. 3. Neighbors points (circle) of γ (bullet).

The statements (B) and (C) always hold for the directional local scales (3) and (4). In fact, note that, if $\gamma \in \Lambda^\ell$, $0 \le \ell \le j-1$, then, by definition, $a_r^j(\gamma) \le \Delta_r^{\ell+1}$, and condition (C) holds. Condition (B) is always true for $\gamma \in X^0 \subset \Gamma^q$, independently of q. For $\gamma \in \Lambda^\ell$, $0 \le \ell \le j-1$, we know that $\Delta_r^q = a_r^j(\gamma) \le \Delta_r^{\ell+1}$. This implies that $q \ge \ell+1$, i.e., $\gamma \in \Gamma^{\ell+1} \subset \Gamma^q$, and the result is also true for this case.

However, the verification of condition (A) is more subtle and requires more structured grids. For instance, the x-directional local scale (3) does not satisfy the condition (A) for the grid $\Gamma^3 \subset X^3$ in Fig. 2. Indeed, for the point $v \in X^0$, in the center of the grid, $a_x^3(v) = \frac{3}{4}\Delta_x^0$, which can not be represented as Δ_x^q for any $0 \le q \le 3$.

Tree condition

To facilitate the verification of condition (A), let us consider grids having a tree structure as follows. A grid Γ^j satisfies the tree condition if for $0 \le \ell \le j-1$:

(a) for a point $\gamma \in \Lambda^\ell$ of the form $\gamma = ((2k+1)\Delta_x^{\ell+1}, 2m\Delta_y^{\ell+1})$, then the two neighbors in $X^\ell\gamma = (k\Delta_x^\ell, m\Delta_y^\ell)$ and $\gamma = ((k+1)\Delta_x^\ell, m\Delta_y^\ell)$ are in Γ^j (see Fig. 3 left).

(b) for a point $\gamma \in \Lambda^\ell$ of the form $\gamma = (2k\Delta_x^{\ell+1}, (2m+1)\Delta_y^{\ell+1})$, then the two neighbors in $X^\ell\gamma = (k\Delta_x^\ell, m\Delta_y^\ell)$ and $\gamma = (k\Delta_x^\ell, (m+1)\Delta_y^\ell)$ are in Γ^j (see Fig. 3 right).

Lemma 2. *For a grid Γ^j satisfying the tree condition, the directional local scales defined in (3) and (4) satisfy the local scale conditions (A–C).*

Proof. As observed before, it only remains to prove condition (A). Let us consider first the case $r = x$. We note that if the result is not true for some $\gamma \in \Gamma^j$, then there is some $\eta = (\eta_x, \gamma_y) \in \Gamma^j$ such that $a_x^j(\gamma) = |\gamma_x - \eta_x| < \Delta_x^q$, where $q = 0$ for $\gamma \in X^0$, and $q = \ell+1$ for $\gamma \in \Lambda^\ell$, $0 \le \ell \le j-1$. We first consider the case $\gamma \in X^0$. Therefore, η can not be a point in X^0. Furthermore, since $\eta_y = \gamma_y$, then $\eta \in \Lambda^q$, $q \ge 0$ has the form $((2k+1)\Delta_x^{q+1}, 2m\Delta_y^{p+1})$. By the tree condition (a), the two neighbors (kh_x^p, mh_y^p) and $((k+1)h_x^q, mh_y^q)$ are in Γ^j. Since one of them must coincide with γ, we obtain that $a_x^j(\gamma) = |\gamma_x - \eta_x| = \Delta_x^p$. Similarly, if $\gamma \in \Lambda^\ell$, $\ell \ge 0$, then η can not be a point in $\Gamma^{\ell+1}$. Recalling that $\eta_y = \gamma_y$, we see that η must has the form $((2k+1)\Delta_x^{p+1}, 2m\Delta_y^{p+1})$, for some $p > \ell$. Again, by the tree condition (a), the two neighbors (kh_x^p, mh_y^p) and $((k+1)\Delta_x^q, m\Delta_y^q)$ are in Γ^j, and one of them must coincide with γ. Therefore, we obtain that $a_x^j(\gamma) = |\gamma_x - \eta_x| = \Delta_x^p$. The proof for the case $r = y$ is similar, where the tree condition (b) is used. □

The grid Γ in Fig. 2 is an example of a grid that does not have the tree structure. For instance, the two points in Λ^2 do not satisfy the tree condition, since at least one of the neighbors in X^2 are not present in Γ.

We observe that the tree structure is a more relaxed restriction than the cone condition, as defined in [4]. Cone like grids are supposed to have a smooth grid density variation. Tree like grids may occur with strong variation in the grid density, as the one indicated in Fig. 4.

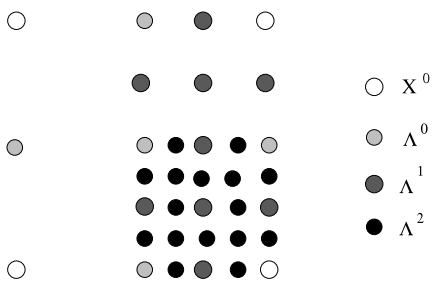

Fig. 4. Example of a tree like grid with strong variation in the grid density.

4. Discretization of derivatives

In this section, the focus is on discretizations of partial derivatives $L^r f = \frac{\partial}{\partial r} f$, $r \in \{x, y\}$, based on the approximation scheme $\mathcal{R}^j(v; f^j)$. For the uniform grid case $\Gamma^\ell = X^\ell$, it is known that interpolatory scaling functions $\phi_\gamma^\ell(v)$ are continuously differentiable [3]. Recall from (1) that $\mathcal{R}^j(v; f^j)$ may be represented as $\mathcal{R}^j(v; f^j) = \sum_{\gamma \in X^j} \tilde{f}_\gamma^j \phi_\gamma^j(v)$, where $\tilde{f}_\gamma^j = \mathcal{R}^j(\gamma; f^j)$. Therefore, the reconstruction operators $\mathcal{R}^j(v; f^j)$ associated with irregular grids inherit the same C^1 smoothness.

Collocation scheme

Given the node values f_γ^j of a function f on the grid Γ^j, the collocation scheme $(L^{r,j} f^j)_\gamma$ is defined as the node values of the partial derivative of the reconstruction $\mathcal{R}^j(.; f^j)$ computed at γ. That is,

$$(L^{r,j} f^j)_\gamma = (L^r \mathcal{R}^j(.; f^j))(\gamma). \tag{5}$$

Using the representation (1), $(L^{x,j} f^j)_\gamma$ may be interpreted as the result of the action of the usual fourth order central finite difference operator

$$\begin{aligned}(L^{x,j} f^j)_\gamma &= \left(L_{FD}^{x,j} \mathcal{R}^j(.; f^j)\right)(\gamma) \\ &= \frac{1}{\Delta_x^j} \sum_k \tilde{f}(\gamma_x - k\Delta_x^j, \gamma_y)\beta(k),\end{aligned} \tag{6}$$

with $\beta(1) = 2/3 = -\beta(-1)$, $\beta(2) = -1/12 = -\beta(-2)$, and $\beta(k) = 0$, $|k| \geq 3$.

Similarly,

$$\begin{aligned}(L^{y,j} f^j)_\gamma &= \left(L_{FD}^{y,j} \mathcal{R}^j(.; f^j)\right)(\gamma) \\ &= \frac{1}{\Delta_y^j} \sum_m \tilde{f}(\gamma_x, \gamma_y - m\Delta_y^j)\beta(m).\end{aligned} \tag{7}$$

Adaptive Formulation: $L_a^{r,j}$, $r \in \{x, y\}$

Holmström [1] introduced the idea of implementing the finite difference schemes (6) and (7) in an adaptive fashion. For each point $\gamma = (\gamma_x, \gamma_y) \in \Gamma^j$ with directional local scales $a_r^j(\gamma)$, define

$$(L_a^{x,j} f^j)_\gamma = \frac{1}{a_x^j(\gamma)} \sum_k \tilde{f}(\gamma_x - k a_x^j(\gamma), \gamma_y)\beta(k), \tag{8}$$

$$(L_a^{y,j} f^j)_\gamma = \frac{1}{a_y^j(\gamma)} \sum_m \tilde{f}(\gamma_x, \gamma_y - m a_y^j(\gamma))\beta(m). \tag{9}$$

In view of Eqs. (6) and (7) at level q, and assuming that the directional local scales $a_r^j(\gamma)$ satisfy the conditions (A–C), these adaptive finite difference formulae can be formulated as adaptive collocation schemes.

Lemma 3. *Suppose that for points in Γ^j we have defined directional local scales $a_r^j(\gamma)$ satisfying conditions (A–C). If $\gamma \in \Gamma^j$, and $a_r^j(\gamma) = \Delta_r^q$, then $(L_a^{r,j} f^j)_\gamma$ can be formulated as*

$$(L_a^{r,j} f^j)_\gamma = \left(L_{FD}^{r,q} \mathcal{R}^q(.; f^q)\right)(\gamma) = \left(L^r \mathcal{R}^q(.; f^q)\right)(\gamma). \tag{10}$$

As we will see below, the adaptive schemes $L_a^{r,j} f^j$ may coincide with their non adaptive versions $L^{r,j} f^j$.

Theorem 4. *Assume that for points $\gamma \in \Gamma^j$ directional local scales are defined satisfying (A–C). Then, the adaptive formulation $(L_a^{r,j} f^j)_\gamma$ coincides with its non adaptive version $(L^{r,j} f^j)_\gamma$ at the points $\gamma \in \Gamma^j$.*

Proof. Let $\gamma \in \Gamma^j$ with $a_r^j(\gamma) = \Delta_r^q$, $q \leq j$. Lemma 1 assures that $\mathcal{R}^q(.; f^q)$ and $\mathcal{R}^j(.; f^j)$ coincide on the stencil points required for the evaluation of $L^{r,j}$ at γ. This means that

$$[L^{r,j}\mathcal{R}^q(.; f^q)](\gamma) = [L^{r,j}\mathcal{R}^j(.; f^j)](\gamma).$$

But, since $\gamma \in \Gamma^q$,

$$[L^{r,j}\mathcal{R}^q(.; f^q)](\gamma) = [L^{r}\mathcal{R}^q(.; f^q)](\gamma) = [L^{r,q}\mathcal{R}^q(.; f^q)](\gamma).$$

Therefore, according to the equivalent adaptive collocation formulation of Lemma 3, we obtain

$$(L_a^{r,j} f^j)_\gamma = [L^{r}\mathcal{R}^q(.; f^q)](\gamma) = [L^{r,j}\mathcal{R}^q(.; f^q)](\gamma) = [L^{r,j}\mathcal{R}^j(.; f^j)](\gamma) = (L^{r,j} f^j)_\gamma. \quad \square$$

Consistency analysis

Let $L_{FD}^{r,j}$, $r \in \{x, y\}$ be the uniform finite difference operators as in (6) and (7). Given the samples f^j of a function in a grid Γ^j, consider the functions $g^r(\nu)$ obtained by the application of $L_{FD}^{r,j}$ on the reconstruction $\mathcal{R}^j(., f^j)$:

$$g^r(\nu) = [L_{FD}^{r,j}\mathcal{R}^j(., f^j)](\nu).$$

For a refined grid $\hat{\Gamma}^j$ containing Γ^j, let $\hat{g}_\gamma^r = [L_a^{r,j}\tilde{f}^j](\gamma)$, $\gamma \in \hat{\Gamma}^j$ be the result of applying the adaptive difference scheme based on $\hat{\Gamma}^j$. We are interested in the error TE^r in approximating g^r by the interpolation of $\hat{g}^r$. That is,

$$TE^r(\nu) = g^r(\nu) - \mathcal{R}^j(\nu; \hat{g}^r).$$

If we see the finite difference operator $L_{FD}^{r,j}$ as playing the role of the r–partial derivative, then TE^r can be interpreted as *the difference between the r–partial derivative of the reconstruction and the reconstruction of the adaptive discrete r–partial derivative*. In this sense, we call TE^r the *truncation error*.

The contributions to this truncation error come from two sources.

- For points $\gamma \in \hat{\Gamma}^j$, $TE^r(\gamma)$ is the difference between $g^r(\gamma)$, which represents the r–derivative computed by the FD scheme using the spacing of finest scale level, and $\hat{g}_\gamma^r$, which is the result of using the FD with local directional scale. As stated in the previous section, this error can be avoided for fourth order schemes if for points in $\hat{\Gamma}^j$ the directional local scales satisfy the conditions (A–C). Precisely, as a consequence of Theorem 4, g^r coincides at $\gamma \in \hat{\Gamma}^j$ with the adaptive finite difference values $\hat{g}_\gamma^r = [L_a^j \hat{f}^j](\gamma)$. This means that $TE^r(\gamma) = 0$ for all $\gamma \in \hat{\Gamma}^j$.
- Assuming that the truncation error vanishes at $\hat{\Gamma}^j$, then $TE^r(\gamma)$ gives the interpolation errors of g^r at points $\gamma \notin \hat{\Gamma}^j$, that is, the wavelet coefficients of g^r. So, the question is what can be said about the wavelet content of g^r outside $\hat{\Gamma}^j$. According to (2), $\mathcal{R}^j(\nu; f^j)$ only contains contributions of wavelets ψ_ν^l, $\nu \in \Gamma^j$. However, differentiation is an action that activates some other wavelets. Thus, components $\psi_\gamma^l(\nu)$, with $\gamma \in X^j \setminus \Gamma^j$, may be present in $g^r(\nu)$. Thus, given a precision $\varepsilon > 0$, the goal of the refinement process is try to construct $\hat{\Gamma}^j$ to guarantee that $|TE^r(\gamma)| < \varepsilon$ for $\gamma \in X^j \setminus \hat{\Gamma}^j$.

As analysed in [7], in the context of multiresolution for cell averages, one may expect that the second kind of perturbation error can actually be controlled by a special refinement strategy for the construction of $\hat{\Gamma}^j$. In the context of interpolatory multiresolution analyses, this subject deserves further studies.

5. Numerical example

Our purpose here is to analyse the performance of the SPR discretization of spatial partial derivatives using either local directional scales or the grid spacing of the finest scale level. As illustrating example, we consider the functions to be analysed as numerical solutions of the TE mode system of Maxwell's equations for the components of the electrical $\mathbf{E} = (E^x, E^y, 0)$ and magnetic $\mathbf{H} = (0, 0, H^z)$ fields

$$\mu \frac{\partial H^z}{\partial t} = \frac{\partial E^x}{\partial y} - \frac{\partial E^y}{\partial x},$$
$$\epsilon \frac{\partial E^x}{\partial t} = \frac{\partial H^z}{\partial y},$$
$$\epsilon \frac{\partial E^y}{\partial t} = -\frac{\partial H^z}{\partial x},$$

where ϵ is the electrical permittivity and μ is the magnetic permeability for the free space. We restrict the problem to the computational domain $[0, 1] \times [0, 1]$, and Perfectly Electrical Conducting (PEC) boundary conditions are enforced,

meaning that the tangential electric field components vanish at the walls, i.e., $E^y(0, y, t) = E^y(1, y, t) = 0$ and $E^x(x, 0, t) = E^x(x, 1, t) = 0$ for all $0 \leq x, y \leq 1$ and $t > 0$. At $t = 0$, the initial conditions are $H^z(x, y, 0) = e^{-3500(x-\frac{1}{2})^2} e^{-3500(y-\frac{1}{2})^2}$, and $E^x(x, y, 0) = E^y(x, y, 0) = 0$.

Both fields **E** and **H** are sampled at the same uniform grid X^j, with spacing $\Delta_x^j = \Delta_y^j = 2^{-j}$. The fourth order FD scheme is applied for the discretization of spatial derivatives. Since some extra virtual FD stencils outside the boundary are required, we use the anti-symmetry properties for E^y at $x = 0$ and $x = 1$, and for E^x at $y = 0$ and $y = 1$. Consequently, symmetry properties are assumed for the magnetic field at all boundary faces. During a time step $n\Delta t \leq t \leq (n+1)\Delta t$, the integration in time uses a first order Euler scheme for which the components of the electrical field are taken at the initial time level $n\Delta t$ to obtain the magnetic field at the next time level $(n+1)\Delta t$. Then, the magnetic field at $(n+1)\Delta t$ is used for the evolution of the electrical field. To ensure stability and to get accuracy, the time step is constrained by the formula $\Delta t = 0.35 \times \sqrt{\mu\epsilon} \times 2^{-j}$. Such scheme is a generalization of the well known FDTD algorithm [8], in the sense that non-staggered grids are used in place of staggered ones and a fourth order spatial FD scheme replaces the low order one of Yee's scheme. We refer to [9] for detailed dispersion and stability analysis of such a reference scheme as well as for 1D SPR simulations.

The plots in Fig. 5 (left) correspond to simulation results for the magnetic field at three different times (ns) $t_1 = 0.009$, $t_2 = 0.584$, and $t_3 = 0.876$ with a uniform grid corresponding to $j = 7$. On the right side of this figure we show the SPR of such fields, using cubic subdivision interpolation, by thresholding the wavelet coefficients with the parameter $\varepsilon_H = 10^{-4}$. It can be observed that the SPR grids are non uniformly sampled, with density varying according to the evolution of the field.

For these instances of the magnetic field, we compute the two contributions to the truncation error for the SPR derivative L^x. Namely, at each point of the sparse grid, we first evaluate the information of the error coming from the difference of discretizations

$$\max_{\gamma}\{|(L^{x,j}f)(\gamma) - (L_a^{x,j}f)(\gamma)|\}, \tag{11}$$

corresponding to applying the FD operator either with the uniform grid spacing of the finest scale level or using the local directional scales. We test this error for the grid obtained after the enforcement of the tree structure and for the grid given by a refinement operation. Being sure that this difference of the SPR derivatives is negligible at all points in the sparse grid, next we evaluate the contribution to the truncation error at the points elsewhere.

For the first contribution, the error is computed after the enforcement of the grid tree structure using the directional local scale (3). As a consequence of Lemma 2, and in accordance with the statement of Theorem 4.1, we observe, within machine precision, a zero truncation error. For comparison, we also consider local directional scales for $\gamma = (\gamma_x, \gamma_y) \in \Gamma^j$ by just taking

$$a_x^j(\gamma) = \min\{|\gamma_x - \eta_x|, \eta = (\eta_x, \gamma_y) \in \Gamma^j, \eta \neq \gamma\}, \tag{12}$$

which do not satisfy the hypotheses (A–C) for general tree like grids. For this form of directional local scale, we observe a significant truncation error of order 10^{-1}.

Next we consider similar tests applied to refined grids. For these applications, we use the refinement procedure adopted in [1] that for each point γ in Γ^j corresponding to a significant wavelet coefficient, i.e. $\gamma \in \Lambda^{\ell-1}$, $0 \leq \ell \leq j-1$, its closest eight neighbors in X^ℓ are included to form a refined grid $\hat{\Gamma}^j$. Furthermore, if $\ell < j$, then its closest eight neighbors in $X^{\ell+1}$ are also included in $\hat{\Gamma}^j$. This refinement procedure is illustrated in Fig. 6, where the original grid is formed by the coarsest grid X^0 and one point $\gamma \in \Lambda^2$. To form the refined grid, the sixteen neighbors of this point γ are included, eight from X^3 and eight from X^4. For the refined grids associated to three time instances of the magnetic field, the differences (11) are also zero within machine precision, independently of the directional local scales used as step size. For this example, one observes that the sparse grids that come after the thresholding and refinement operators naturally hold the directional tree structure. Furthermore, both formulae for the directional local scale, (3) and (12), coincide.

Table 1 shows the percentage of points, with respect to the uniform grid in the finest scale level, present in each of the sparse grids, either after the enforcement of the tree structure or the refinement operation. At the beginning, since the features of the magnetic field are highly concentrated around the initial pulse, there is a large amount of data compression. As time evolves, the circular wave front spreads towards the boundary, requiring more points to be represented. As expected, the SPR refined grids are more numerous than the grids obtained by just enforcing the tree structure. This table also displays the number of interpolations used in the computation of the SPR derivatives using the directional local scale (3) expressed as a percentage of the number of interpolations required to compute the derivatives using the step size of the finest scale level. In both studies, the savings in interpolations range from 87% to 70%, for the tree like SPR grids, and from 88% to 73%, for the refined SPR grids, the gain being more significant at the beginning of the simulation, when the grids have more sparsity.

Being sure that using the directional local scale (3) the resulting truncation error is practically zero at the points of the sparse grids holding the tree structure, either with or without refinement, we turn to the analysis of the error contributions at points located elsewhere.

We recall from Section 4 that outside the grid where the SPR derivative is evaluated the truncation error represents the wavelet coefficients of the function $L_{FD}^{x,j}\mathcal{R}^j(., Hz^j)(\nu)$. Our purpose is to evaluate the efficiency of the refinement procedure in capturing a good SPR for this derivative of the magnetic field. The results of such consistency analysis are presented in Table 2, for tree like grids without refinement, and in Table 3, after the refinement operation. In both cases, we extend the

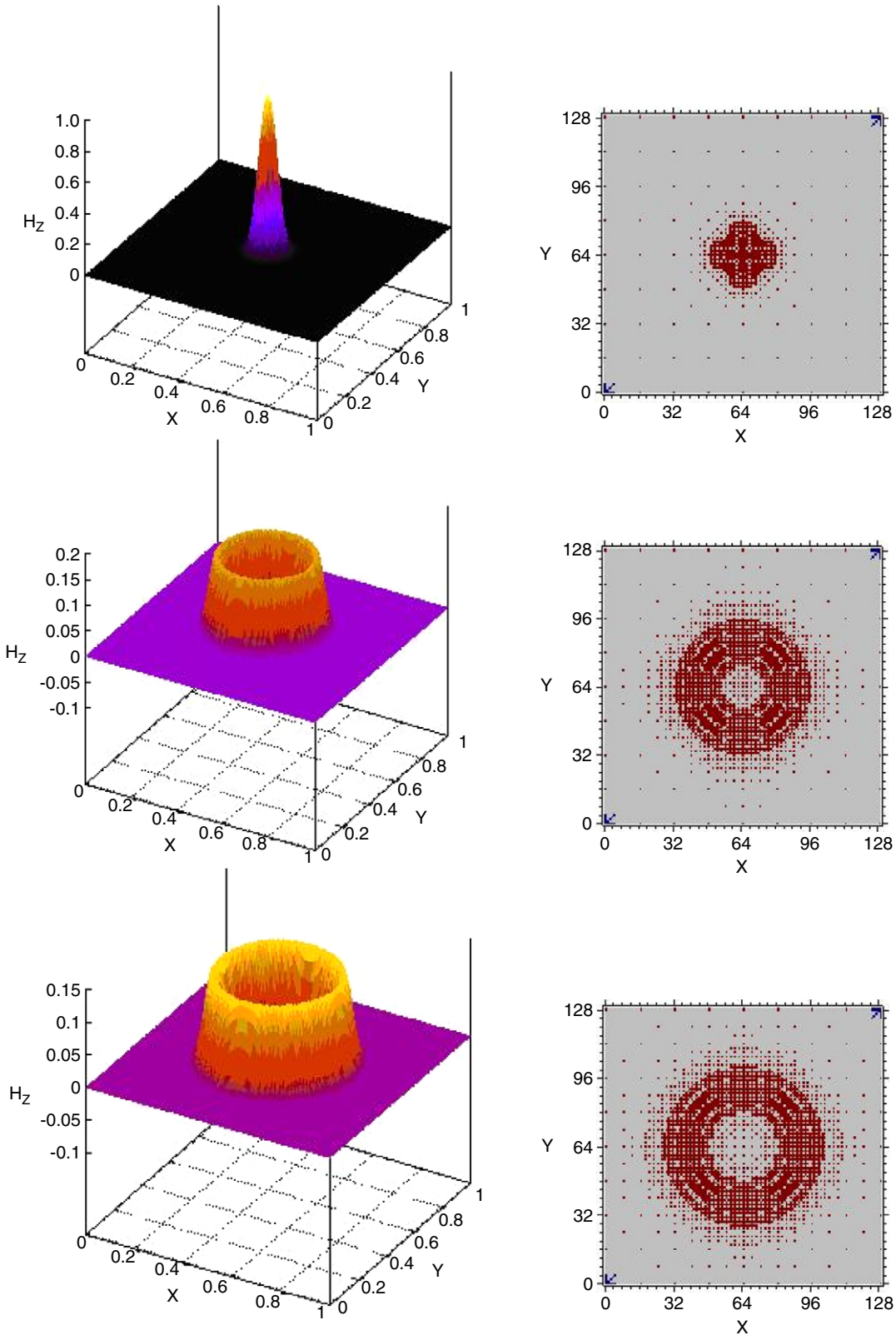

Fig. 5. Time evolution of the magnetic field (left) and the corresponding SPR grid (right) for $\varepsilon = 10^{-4}$, at times (ns) $t_1 = 0.009$, $t_2 = 0.584$ and $t_3 = 0.876$.

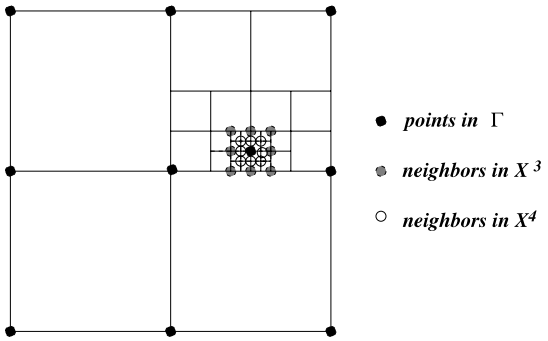

Fig. 6. Illustration of the refinement process: Γ is formed by the coarsest grid X^0 and one point $\gamma \in \Lambda^2$. The refined grid $\hat{\Gamma}$ is formed by adding to Γ the sixteen neighbors of this point γ, eight from X^3 and eight from X^4.

Table 1
Percentage of used points and interpolations for the computation of SPR derivative after the enforcement of the tree condition and refinement.

Time	With tree condition (%)		With refinement (%)	
	Used points	Interpolations	Used points	Interpolations
t_1	5	13	9	12
t_2	17	25	33	21
t_3	23	30	50	27

Table 2
Truncation error in SPR derivatives: tests for tree structured grids without refinement.

Time	Tree structure			
	$j = 7$		$j = 8$	
	TE error	# points	TE error	# points
$\varepsilon_H = 10^{-3}$				
t_1	5.400440×10^{-1}	381	5.598303×10^{-1}	381
t_2	4.958390×10^{-1}	821	5.239063×10^{-1}	821
t_3	5.431991×10^{-1}	1109		1 117
			5.425516×10^{-1}	
$\varepsilon_H = 10^{-4}$				
t_1	19.27483×10^{-2}	765	12.37215×10^{-2}	1 037
t_2	6.279617×10^{-2}	2757	6.329703×10^{-2}	2 749
t_3	5.862434×10^{-2}	3873		3 913
			6.184630×10^{-2}	
$\varepsilon_H = 10^{-5}$				
t_1	10.29540×10^{-3}	1157	11.87374×10^{-3}	2 509
t_2	8.507794×10^{-3}	4577	8.576567×10^{-3}	9 501
t_3	31.28736×10^{-3}	6525	23.81233×10^{-3}	13 325

analysis by considering $j = 7$, and $j = 8$, and letting the thresholding parameter be $\varepsilon_H = 10^{-3}$, 10^{-4} and 10^{-5}. As expected, a comparison of the results in both tables reveal that the refinement operation helps to reduce the truncation error, at the cost of less sparsity. However, the ratio TE_{wr}/TE_r, of the truncation error without refinement and the truncation error with refinement, seems to be greater than the ratio NP_r/NP_{wr}, of the number of points in the refined grid and the number of points before refinement.

The plots in Fig. 7 illustrate this behavior for the magnetic fields at $t = t_1$ (top) and $t = t_3$ (bottom), for the variation of the threshold parameter ε_H between 10^{-5} to 10^{-3}. For instance, we conclude from the curves in the top-left part, for SPR grids at $j = 7$ for the magnetic field at $t = t_1$, that the refinement doubles the number of points but the truncation error without refinement can be 15 to 30 times larger, especially for $\varepsilon_H < 7 \times 10^{-4}$. At higher resolution $j = 8$, the curves in the top-right part of Fig. 7 show that the gain in the truncation error double-compensates the increase in the number of points in the refined grid, for $\varepsilon \geq 10^{-4}$. For smaller thresholding parameters $\varepsilon < 5 \times 10^{-5}$, the impact of refinement is again very important in reducing the truncation error with low cost in the additional number of points. A similar trend is verified for the field at $t = t_3$, as we can see in Fig. 7 (bottom), both for $j = 7$ (left) and $j = 8$ (right). These plots show that for larger thresholding parameters there is a balance in the reduction of the truncation error with the increase of the number of points in the refined grids. For smaller values of ε_H, the gain in the truncation error with refinement can be very significant, up to 40 or 12 times larger than without it, for $j = 7$ and 8, respectively, with very low extra cost.

The plots in Fig. 8 represent the normalized truncation error $TE/(100 \times \varepsilon_H)$ for the Hz field at $t = t_1$ (left) and $t = t_3$ (right). Since the truncation error represents the wavelet coefficients of the function $L_{FD}^{x,j}\mathcal{R}^j(.,\ Hz^j)(\nu)$, the conclusion drawn

Table 3
Truncation error in SPR derivatives: tests for grids after refinement.

Time	Refined grid			
	$j = 7$		$j = 8$	
	TE error	# points	TE error	# points
$\varepsilon_H = 10^{-3}$				
t_1	0.9880369×10^{-1}	1018	$1.087488e \times 10^{-1}$	1 597
t_2	1.223386×10^{-1}	1933	1.297945×10^{-1}	2 622
t_3	1.510714×10^{-1}	3437	1.845292×10^{-1}	3 625
t_4	1.224536×10^{-1}	5128		5 154
			1.482000×10^{-1}	
$\varepsilon_H = 10^{-4}$				
t_1	0.6293835×10^{-3}	1485	2.812171×10^{-2}	3 332
t_2	2.738631×10^{-2}	3118	2.305200×10^{-2}	6 849
t_3	0.9277954×10^{-2}	5552	1.877493×10^{-2}	12 585
t_4	1.380015×10^{-2}	8241		18 203
			1.754093×10^{-2}	
$\varepsilon_H = 10^{-5}$				
t_1	0.7332167×10^{-3}	1990	1.116536×10^{-3}	5 005
t_2	0.7992242×10^{-3}	3817	1.116536×10^{-3}	10 769
t_3	0.7992242×10^{-3}	6516	2.181932×10^{-3}	20 178
t_4	0.8040323×10^{-3}	9964	1.926749×10^{-3}	29 610

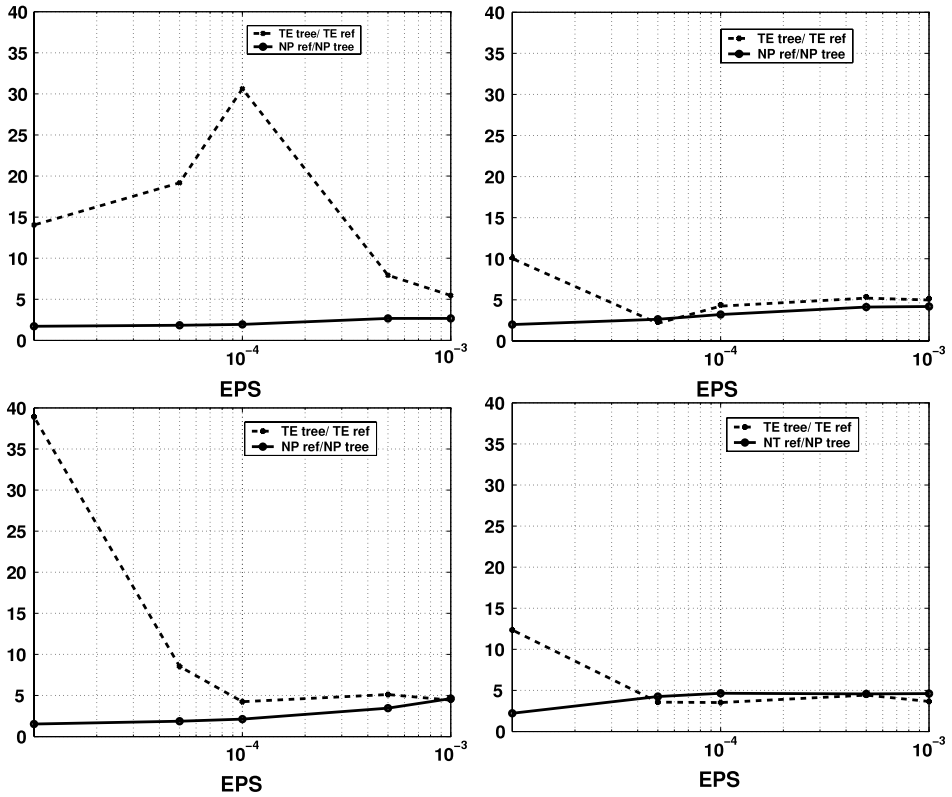

Fig. 7. Comparison of truncation error and grid densities, in terms of the threshold parameter ε_H, for tree like grids with and without refinement: $j = 7$ (left), $j = 8$ (right); $t = t_1$ (top), $t = t_4$ (bottom).

from these plots is that, after the refinement of the ε_H–SPR of the magnetic field, we obtain a ε_E-SPR for its x–derivative, where $\varepsilon_E \approx 100 \times \varepsilon_H$.

6. Concluding remarks

In this paper we consider adaptive fourth order finite difference schemes $L_a^{r,j} f^j$, for partial derivatives in the $r = x$ and $r = y$ directions, arising in the bidimensional SPR method. The information f^j is formed by point values in a sparse

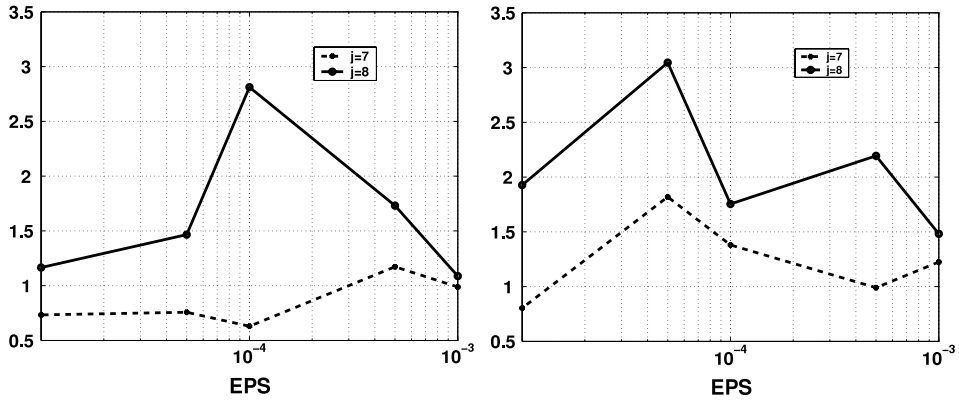

Fig. 8. Normalized truncation error $TE/(100 \times \varepsilon_H)$ in terms of the threshold parameter ε_H; $t = t_1$ (left), $t = t_4$ (right).

grid adapted to the function under consideration, and the main principle is to approximate directional derivatives by uniform finite differences, using a step size proportional to each point local scale $d_r^j(\gamma)$ in the corresponding direction of differentiation. Required neighboring stencils that are not present in the adaptive grid are interpolated by means of a reconstruction operator. The main results of our study are:

- To preserve accuracy in such adaptive discretizations, the grid structure and the form of the directional local scales are important. Under the conditions stated in (A–C), we prove a statement for the local behavior of the reconstruction operator. This crucial result is the basis for the proof of Theorem 4.1 that guaranties that the adaptive SPR discretizations $L_a^{r,j} f^j$ coincide at the points of the adaptive SPR grid with their non adaptive formulations $L^{r,j} f^j$, where the step size corresponds to the spacing of the finest scale level. This result is favorable to applications of the SPR method, in terms of the number of operations to be done. In fact, the formulations $L_a^{r,j} f^j$ are more economical than $L^{r,j} f^j$, since they do not require the calculation of the stencils up to the most refined level, for those points having large local scales $d_r^j(\gamma) \gg \Delta_r^j$.
- A grid tree structure and directional local scales $d_r^j(\gamma)$ are defined satisfying conditions (A–C).
- Furthermore, the consistency analysis indicates that, in order to keep the truncation error under a certain given precision, an adequate refinement strategy should be used.

Numerical tests are presented for functions representing magnetic fields occurring in the simulation of the Maxwell equations. The numerical consistency analysis for such examples reveals that the structure of the grids that come from the application of the thresholding and refinement operators are sufficient to ensure a small truncation error. In fact, for the experiments of the present paper, the tree structure naturally holds for the SPR refined grids, which ensures that the adaptive SPR finite difference schemes $L_a^{r,j}$ can be safely applied. However, in general SPR, the grids obtained after thresholding and refinement operations may not have the tree structure. Therefore, before the application of adaptive SPR finite difference schemes $L_a^{r,j}$, the enforcement of the tree structure after refinement is recommended.

For further reading

[10].

Acknowledgements

The research of this paper is part of a scientific international cooperation between GRICES (Portugal) and CAPES (Brazil) (contract 142/05). This research has also been partially supported by CNPq (contracts 308632/2006-0 and 308680/2007-3) and FAPESP (Brazil) (contracts 2004/06880-3, 2007/52015-0).

References

[1] M. Holmström, Solving hyperbolic PDEs using interpolating wavelets, SIAM Journal of Scientific Computing 21 (1999) 405–420.
[2] S.M. Gomes, B. Gustafsson, Combining wavelets with finite differences: a consistence analysis, Technical Report 2002-001, Uppsala University, 2002.
[3] G. Deslauriers, S. Dubuc, Symmetric iterative interpolation processes, Constructive Approximation 5 (1989) 49–68.
[4] F. Plantevin, Wavelets on irregular meshes, Advances in Computational Mathematics 4 (1995) 293–329.
[5] D. Donoho, Interpolating wavelet transform, Technical Report 408, Dept. of Statistics, Stanford University, 1992.
[6] M.K. Kaibara, Análise de Multi-resolução para Leis de Conservação em Malhas Adaptativas, Ph.D Thesis. IMECC-Unicamp, Brazil, 2000.
[7] A. Cohen, S.-M. Kaber, S. Müller, M. Postel, Fully adaptive multiresolution finite volume schemes for conservation laws, Mathematics of Computation 72 (2002) 183–225.
[8] A. Taflove, Computational Electrodynamics: The Finite-Difference Time-Domain Method, Norwood, MA, 2000.
[9] P. Pinho, M.O. Domingues, P.J. Ferreira, S.M. Gomes, A. Gomide, J.R. Pereira, Interpolation wavelets and adaptive finite difference schemes solving Maxwell's equations: the effects of gridding, IEEE Transactions in Magnetics 43 (2007) 1013–1022.
[10] I. Daubechies, Ten Lectures on Wavelets, SIAM (1992).